Published in final edited form as:
Brain Stimul. 2009 October 1; 2(4): 215–228. doi:10.1016/j.brs.2009.03.007.

Role of Cortical Cell Type and Morphology in Sub- and Suprathreshold Uniform Electric Field Stimulation

Thomas Radman[1,*], **Raddy L Ramos**[2], **Joshua C Brumberg**[3], and **Marom Bikson**[1]

[1] Department of Biomedical Engineering, City College of the City University of New York, New York, New York

[2] Department of Neuroscience, New York College of Osteopathic Medicine NYIT, Old Westbury NY

[3] PhD Department of Psychology, Queens College, CUNY, Flushing, New York

Abstract

Background—The neocortex is the most common target of sub-dural electrotherapy and non-invasive brain stimulation modalities including transcranial magnetic stimulation (TMS) and transcranial current simulation (TCS). Specific neuronal elements targeted by cortical stimulation are considered to underlie therapeutic effects, but the exact cell-type(s) affected by these methods remains poorly understood.

Objective—We determined if neuronal morphology or cell type predicted responses to sub- and suprathreshold uniform electric fields.

Methods—We characterized the effects of sub- and supra-threshold electrical stimulation on identified cortical neurons *in vitro*. Uniform electric fields were applied to rat motor cortex brain slices, while recording from interneurons and pyramidal cells across cortical layers, using whole cell patch clamp. Neuron morphology was reconstructed following intracellular dialysis of biocytin. Based solely on volume-weighted morphology, we developed a parsimonious model of neuronal soma polarization by sub-threshold electric fields.

Results—We found that neuronal morphology correlated with somatic sub-threshold polarization. Based on neuronal morphology, we predict layer V pyramidal neuronal soma to be the most sensitive to polarization by optimally oriented sub-threshold fields. Supra-threshold electric field action potential threshold was shown to reflect both direct cell polarization and synaptic (network) activation. Layer V/VI neuron absolute electric field action potential thresholds were lower than Layer II/III pyramidal neurons and interneurons. Compared to somatic current injection, electric fields promoted burst firing and modulated action potential firing times.

Introduction

Clinical application of transcranial magnetic stimulation (TMS) and transcranial current stimulation (TCS, encompassing transcranial direct current stimulation (tDCS), cranial electrotherapy stimulation, transcranial electric stimulation (TES), and electroconvulsive therapy) are promising non-invasive approaches for the treatment of a number of psychiatric,

[*]Corresponding Author: 140th Street and Convent Avenue, CCNY BME, Steinman Hall Room T-463, New York, NY 10031, Phone: 718.749.6808, tradman00@ccny.cuny.edu.

neurological, and pain disorders [1–6] as well as the study of human cognitive function and neural plasticity [7–10]. Because the electric field (voltage gradient in the extracellular space induced in the brain by TMS/TCS decays with distance from the stimulating coil or electrode, the neocortex is the most common target of non-invasive electrotherapy [11–15]. Invasive cortical stimulation using sub-dural strips/arrays is indicated for a range of therapeutic and diagnostic applications including pain and pre-operative brain mapping [16,17].

Fundamental questions remain regarding the cellular targets of each cortical stimulation paradigm, including the relative activation of morphologically and functionally diverse groups of inhibitory interneurons and excitatory pyramidal cells [18]. Stimulation waveform, direction, and frequency is thought to preferentially affect specific cortical cell types [18–20] and/or specific segments of a neuron such as axonal bends and terminations [11,21,22]. Neuronal segments oriented toward the stimulating anode (virtual anode for electric fields induced by TMS [22]) have been shown to hyperpolarize, and concomitantly the segments oriented toward the (virtual) cathode depolarize (Supplementary Fig. 1) [23,24].

The effects of electric field-induced polarization has traditionally been categorized as “subthreshold” changes in ongoing neuronal processing/timing [25–27], or “suprathreshold” stimulation that directly triggers action potentials [26,28,29]. Clinical brain stimulation modalities, and associated therapeutic outcomes, may depend specifically on subthreshold (e.g. tDCS) and/or suprathreshold (e.g. TMS) neuronal effects (see [30] for review). Cortical cell types [31], distinguished by their laminar position, network connectivity, and neuronal morphology/biophysics, play defined roles in network processing and thus merit investigation in the context of both sub- and suprathreshold stimulation paradigms [18].

In response to the unique electric fields induced by each brain stimulation modality [22,32–34], neuronal membranes are considered to polarize in a “compartment” specific manner; the polarized compartments interact according to the electrotonic decay along the neuron (Supplementary Fig. 1). Neuronal modeling [35–38] and *in vitro* [25,39] studies of electric field stimulation have identified morphological features which govern the polarization of (interacting) neuronal compartments, including branching patterns and membrane space constants. Changes of compartment angle relative to an applied electric field (e.g. activating function, the 2^{nd} derivative of the extracellular voltage along the neuronal membrane), branch terminations, or changes in inter-compartment impedance can determine the locations of entry and exit of induced transmembrane currents that lead to polarization [21,25,35,38,40]. The neuronal space constants (λ), and related diameter of axons and dendrites, govern the axial distribution of these induced transmembrane polarizations, and therefore regulate the degree to which neuronal compartments interact [38,39,41,42]. Concurrent polarization of individual segments of a neuronal tree can lead to complex changes in overall neuronal function by modulating cellular biophysics [43,44] including non-linear voltage-gated conductances, synaptic efficacy, and AP threshold or timing [23,28,29,45,46].

The goal of the present study was to determine if the distinct morphological features of cortical cell types affect their response to stimulation by electric field. We performed whole-cell recordings, of pyramidal cells and interneurons in rat motor cortex brain slices, during uniform electric field stimulation *in vitro*. Morphological reconstructions of biocytin-filled neurons were correlated with electrophysiological responses to electric fields. We considered differences between cortical cell types in their response to both subthreshold and suprathreshold stimulation. These data were used to analyze the cellular targets of clinical cranial stimulation therapies.

Methods

Brain Slice Preparation

Coronal slices (300 μm) of primary motor cortex (M1) were prepared from male P21-25 Sprague-Dawley rats on a vibratome (Integraslice 7550 PSDS, Campden Instruments, Lafeyette, Indiana, USA) as previously described [25,47–49]. In brief, rats were anaesthetized with intraperitoneal ketamine (7.4 mg/kg) and xylazine (0.7 mg/kg) and euthanized by decapitation. Following decapitation, the brain was quickly removed, blocked, and placed into ice-cold (4°C) oxygenated artificial cerebral spinal fluid (ACSF). ACSF contained (in mM) 125 NaCl, 26 $NaHCO_3$, 3 KCl, 1.6 $CaCl_2$, 1.5 $MgS0_4$, 1.25 NaH_2PO_4, and 10 glucose, aerated with 95% O_2–5% CO_2 to a final pH of 7.4. The slices were stored in a holding chamber submerged in ACSF and bubbled with a mixture of 95% O_2–5% CO_2 at room temperature. After >60 min, slices were transferred to a submerged patch-clamp recording chamber maintained at 36°C.

In some experiments, the glutamatergic transmission blockers CNQX (AMPA receptor antagonist, 20 μM) and APV (NMDA receptor antagonist, 50 μM) were added to the perfusate (Sigma-Aldrich, St. Louis, MO).

Whole cell patch clamp recording and data acquisition

Conventional whole-cell patch clamp recording techniques were used to measure activity from neurons in M1. Neurons were visualized with IR-DIC illumination (Olympus BX51WI, Center Valley, PA, USA), and identified according to layer and gross morphology. Patch pipettes (~4–7 MΩ tip resistance) were pulled on a Flaming/Brown microelectrode puller (P-97, Sutter Instruments, Novato, CA, USA). Pipettes were filled with (in mM) 120 KGlu, 10 NaCl, 20 KCl, 10 HEPES, 2 Mg-ATP, 0.3 Na-GTP, 0.5 EGTA, and 0.3–1% biocytin (wt/vol) for subsequent visualization of the neurons. Electrophysiological signals were amplified (Axoclamp-2B, Molecular Devices, Sunnyvale, CA, USA) and filtered at 10 kHz (FLA-01, Cygnus Technologies, Delaware Water Gap, PA, USA), then digitized (Power 1401 ADC/DAC, Cambridge Electronic Design, Cambridge, UK). Off-line analysis of action potential and passive membrane properties were performed using Signal 3 (Cambridge Electronic Design, Cambridge, UK). Upon obtaining a high resistance seal (> 1 GΩ) with a neuron but prior to establishing whole-cell configuration, the microscope objective (water immersion; 40×, Olympus) was removed from the bath to reduce perfusate level (and related electric field) non-uniformities. Once a stable whole-cell configuration was obtained (resting membrane potential of <−55 mV, overshooting action potentials, generation of repetitive action potentials in response to a depolarizing current pulse), neurons were classified according to discharge pattern in response to a constant depolarizing current pulse (100 ms) as intrinsically bursting, regular spiking, etc. [47,50,51].

Generation of uniform electric fields and quantification of neuronal response

Uniform electric fields were generated across individual slices by passing current between two parallel Ag/AgCl electrodes [25,48,52–56] placed on the bottom of a customized submerged chamber; the wires were parallel to the direction of perfusate flow and measuring 15–16 mm long and 7–9 mm apart. Field waveforms were generated by a Power 1401 ADC/DAC (Cambridge Electronic Design, Cambridge, UK) and converted to a controlled current source by up to three parallel stimulus isolation units (2200, 2300, A-M Systems, Carlsborg, WA, USA). Due to the reduced current density caused by the deeper fluid levels in submerged patch recording chambers, to achieve electric field magnitudes comparable to those applied in previous studies utilizing interface recording chambers [25,48], an order of magnitude greater current intensity was necessary. This, in turn, limited the maximum electric field applied (for example in determining action potential thresholds). The electric field (mV/mm) in the

chamber was measured by two recording electrodes separated by 1 mm and calibrated to the current passed through the Ag/AgCl electrodes. The convention of electric field polarity used in the present report refers to the anode on the pial side of the cortex.

The voltage recorded by a field electrode (placed within 50 μm of the recorded neuron) was subtracted from the intracellular potential to obtain the transmembrane voltage and used to compensate for the exogenous electrical artifact. Post-hoc corrections for voltage differences between the field and intracellular electrode were made by scaling the electric field command waveform to the inter-electrode difference and subtracting from the recorded transmembrane voltage. We note that this creates a residual onset-and offset artifact that was not included in our analysis. For each cell, the somatic steady-state transmembrane voltage response to ~ 5 mV/mm electric field steps (Fig. 2B), up to ~ +/−30 mV/mm, were linearly fit (Fig. 1), the slope of which determined the cell-specific subthreshold somatic polarization per unit electric field applied (Fig. 2C), in units of mV of polarization per mV/mm of electric field (mV*(mV/mm)$^{-1}$). This slope, which has also been referred to here as “mV per mV/mm”, “coupling coefficient” and “cell susceptibility” [25,48,52], reduces to mm, and shall be referred to here as polarization length, λ_p.

Suprathreshold electric fields induced non-linear polarizations with characteristic excitatory post-synaptic potential (EPSP) waveforms [49] and/or action potentials, as determined by visual inspection. Averages are reported as mean +/− standard error. Statistics within a 95% confidence interval have been labeled as significant.

Morphological reconstruction of biocytin-filled neurons

Following recordings, slices were placed in cold fixative (4% paraformaldehyde in 0.1 M phosphate buffer) and kept at 4°C for no more than 2 weeks. Biotin-avidin-HRP histochemistry was performed as previously described [57–59]. Briefly, sections were first placed in 1% H_2O_2/0.5% MEOH in phosphate buffer saline (PBS) in order to quench endogenous peroxidase activity. After 3 washes in PBS, sections were permeabilized for one hour in PBS containing 0.2% Triton-X (Sigma, St. Louis, MO, USA). Sections were then placed in an avidin-HRP mixture (ABC Kit, Vector Labs, Burlingame, CA, USA) for 2 hrs. Following 3 washes in PBS, sections were reacted in 0.05% diaminobenzidine/0.015% H_2O_2. Slices were washed in PBS, mounted onto gelatin coated-slides and coverslipped in DPX (Electron Microscopy Sciences, Hatfield, PA, USA). For three-dimensional morphological reconstructions, the Neurolucida system (MicroBrightfield, Williston, VT, USA) was used in conjunction with an Olympus BX51 microscope using 4× (0.1 numerical aperture (NA)), 10× (0.4 NA) and 60× (1.4 NA, oil) objectives. Digital images were taken using an Optronics Microfire camera (Optronics Inc., Muskogee, OK, USA) attached to a dedicated PC. Morphological measurements were made using the NeuroExplorer software package (MicroBrightfield, Williston, VT, USA). Dendritic morphology was used to indentify cell type and layer. The tracing was aligned so the direction of the electric field traversed along the 90° line from the top of the tracing to the bottom. NeuroExplorer (Microbrightfield, Williston, VT, USA) branched structure analyses were used to measure segment angle (ϕ_{seg}) and volume information for each segment of each individual neuron’s tracing.

Volume-weighted polar histogram generation

The volume of each segment was binned by segment angle in a polar histogram (Fig. 4A–C), and summarized by a single vector of mean angle (degrees) and vector length (volume, μm^3). 90 degrees is defined as pointing towards the anodal electric field stimulating electrode (Fig. 4A–C. Histograms were generated using the Matlab (Mathworks, Natick, MA, USA) Circular Statistics Toolbox by Philip Berens.

DC stimulation strength-time to first spike curves

To determine respective stimulation "DC-chronaxies", the threshold stimulation magnitude in response to incrementing electric field steps of 100 ms duration (functionally DC), as well as to incrementing 100 ms steps of somatic current injection, was plotted against the inverse of the time to first spike. These data were fit to the equation $S=S_o+ S_o C/t$, where S is the threshold stimulation magnitude (in nA for current injection, mV/mm for electric field stimulation), S_o is the rheobase corresponding to the horizontal asymptote of the strength-duration curve, C is the DC-chronaxie equal to the duration of stimulation pulse having twice the intensity of the rheobase, and t is time to first spike in milliseconds [60]. Note "classic" strength duration curves are determined using duration of incrementing stimulation pulse necessary to trigger an action potential [61].

Results

We quantified the acute effects of uniform electric fields on cortical neurons *in vitro*. For the cases of sub-threshold and suprathreshold fields we considered if neuronal responses could be distinguished based on cortical cell type or neuronal morphology. Cortical cell types can be defined by anatomical and biophysical distinctions, while we developed a parsimonious metric of neuronal morphology relative to the orientation of applied uniform fields. In response to subthreshold fields, neuronal compartments polarize linearly with the amplitude of the applied electric field [35,38,40–42]; for each neuron, somatic sub-threshold sensitivity is defined by the polarization length constant: λ_p (in mm). Thus, for a given subthreshold electric field E (in mV/mm), neuronal soma will polarize $E{\cdot}\lambda_p$ mV. The sign of the polarization length reflects the polarity of polarization for a given electric field direction. Suprathreshold fields induce non-linear responses in the cell membrane including action potentials and/or EPSPs from activated afferents. The electric field threshold for triggering an action potential in a given neuron reflects the neuron's specific sensitivity to suprathreshold fields. The main objective of this study was to determine if sub- and suprathreshold sensitivities to electric fields could be correlated with cortical cell type or neuronal morphology.

Cortical cell subthreshold polarization in response to uniform electric fields

A total of 51 neurons from M1 were recorded, 37 of which were identified by cortical layer and cell type. Consistent with findings in other structures [23,25], the direction of cortical sub-threshold somatic polarization increased linearly with increasing electric field steps, and reversed polarity with the direction of the applied electric field. Per our convention (see Methods), a 'positive' sub-threshold soma polarization indicated a positive field (anode proximal to pial surface) resulting in membrane depolarization; while a 'negative' sub-threshold polarization indicates a positive field resulting in a membrane hyper-polarization The polarity and polarization sensitivity of each neuronal soma in response to an applied electric field was quantified.

51 cells had a subthreshold transmembrane polarization length, λ_p, ranging from −.29 to .49 mm (such that field-induced subthreshold polarization = $\lambda_p{*}E$ mV, where E is the applied electric field in units of mV/mm). 14 identified layer V/VI (LV/VI) pyramidal cells had a range of polarization lengths, λ_p, from −.03 to .49 mm. The 8 identified layer II/III (LII/III) cells had subthreshold polarization lengths, ranging from −0.05 to 0.13 mm. 15 identified interneurons (from across all layers), had subthreshold polarization lengths ranging from −.29 to .14 mm. These data are thus indicative of the range of possible sub-threshold polarization values for a distributed population of cortical neurons. These polarization ranges are reported without accounting for variable cell angle relative to the electric field, and morphology differences within and across cell types [51,62] (including slicing related damage).

Without accounting for variable cell morphology relative to the electric field, a significant difference was found between the polarization length, λ_p, for interneurons across layers and LV/VI pyramidal neurons ($p < .02$), the difference between interneurons across layers and LII/III pyramidal neurons approached significance ($p = .06$)) (T-test, Fig. 2). Layer V neurons represented the 7 highest (19%) somatic polarization values of the 37 identified cells (Fig. 3).

Neuronal morphology relative to applied electric field correlates to induced subthreshold polarization: volume weighted polar histograms

Volume weighted polar histograms were constructed based on morphological reconstructions of intracellularly recorded neurons (see methods). This reduced representation of individual neuron morphology may be described by a mean angle and vector length (Fig. 4A–C). Mean angle and vector length were significantly correlated to somatic polarization length, λ_p (Fig. 4D, Supplementary Fig. 2, regression model: $\lambda_p = m$*sine(mean angle) * vector length, for each neurons means angle, vector length, and polarization length, where m represents a single scaling variable common to all neurons). The significantly fit plane illustrates the correlation between the asymmetry of neuronal morphology relative to the soma (vector length), modulated by the sine of the mean angle of that morphological projection relative to the electric field, with increasing polarization length (F-statistic=19.52, $p < .001$, $r^2 = .41$, $n = 30$). Neuronal morphologies with mean angles of 0 or 180° (i.e. perpendicular to the electric field) would be represented in the model with polarization lengths of 0 mm (sine(0) = sine(180°) = 0). Mean angles of 90° or 270° degrees would be represented as the optimal orientation relative to the electric field to respectively de- or hyperpolarize the neuron (sine(90°)=1, sine(270°)=−1). Electric field induced AP threshold did not correlate with mean angle and vector length for our sampled cortical neuron population.

If all the neurons we recorded were optimally oriented to the electric field (mean angle = 90°), the regression model would reduce to $\lambda_p \propto$ vector length. A significant difference was found between the vector length for interneurons and both LII/III pyramids ($p \ll .001$) as well as LV/VI pyramidal neurons ($p < .04$) across layers (T-test, Fig. 5).

Cortical cell AP threshold in response to uniform electric fields

The minimum action potential (AP) threshold in response to 100 ms, +/− polarity electric field square pulses was determined (n=26). 3 cells were able to fire in both electric field polarities and the lesser magnitude polarity was considered the “minimum” threshold. 18 of 26 cells had a positive minimum threshold ranging from 28 to 101 mV/mm (mean = 58 +/− 5), and 2 cells had negative minimum thresholds of −80 and −120 mV/mm (mean = −100 +/− 20 mV/mm). 6 cells did not fire an AP in response to the maximum electric field tested in either polarity. No cells fired in response to the offset of the electric field step (e.g. in response to anodic break).

The minimum electric field induced firing threshold for identified LV/VI pyramidal cells ranged from 28 to 72 mV/mm (n=9, mean=49 +/− 6 mV/mm). For LII/III pyramidal neurons, the minimum electric field AP threshold range was 70 to 104 mV/mm (n=6, 81 +/− 5 mV/mm). Thus all identified pyramidal cells had a positive minimum AP threshold. The minimum electric field AP threshold range for interneurons was 44 to 79 mV/mm in the positive direction (n=6, 64 +/− 7 mV/mm), and −80 and −120 mV/mm in the negative direction (n=2, −100 +/− 20 mV/mm) (Supplementary Fig. 3). A significant difference was found between the absolute value electric field firing threshold of LV/VI pyramidal neurons, and both LII/III pyramids ($p < .002$) as well as interneurons ($p < .03$) across layers (T-test, Fig. 6). Note this difference was observed without accounting for variable cell angle relative to the electric field, morphology differences within and across cell types (and slicing related damage), or pre-synaptic contribution.

Increasing intensity of electric field beyond the subthreshold polarization range (see methods) resulted in EPSPs for most cells (n=34) reflecting the activation of action potentials in axons afferent to the specific cortical neuron. This was in distinction to relatively rare EPSPs when electric field stimulation was off. In all but 3 of 26 suprathreshold responding neurons, EPSPs contributed to the depolarization towards AP threshold (Fig. 7). For cells exhibiting EPSPs, the minimum positive electric field value inducing EPSPs ranged from 12 to 69 mV/mm (mean = 49 +/− 4 mV/mm) (n=18). The negative EPSP threshold range was −22 to −104 mV/mm (mean = −62 +/− 7) (n=16). These EPSPs were suppressed by bath application of glutamatergic transmission blockers CNQX and APV (n=4, Fig. 7) consistent with an orthodromic origin. After glutamatergic transmission blockade, action potentials could no longer be triggered in these four cells when stimulated up to the maximal intensity electric field tested (from +/− 79 to 110 mV/mm across these four cells). This analysis underscores the potential contribution of afferent glutamatergic synapses in depolarizing cells to AP threshold, in response to 100 ms electric field pulses.

Stimulation parameters used in TMS and TES are typically short duration pulses less than 1 ms, and can be either monphasic or biphasic. As an initial characterization of the biophysics of cortical cell types in response to stimuli of short duration, we tested the response of 19 cells to brief duration (0.5 ms) square wave electric field stimuli up to the intensity limits of our experimental set-up (ranging from up to 79 to 120 mV/mm). 2 of 19 cells responded to a 0.5 ms square pulse step (mean 88 +/− 8 mV/mm); these cells responded to this 0.5 ms electric field stimuli with a spike ~2 ms after stimulation onset; this short delay is indicative of direct neuronal activation (i.e. the time course excludes synaptic contributions). EPSPs, reflecting orthodromic activation, were observed in another 2 cells at the maximum intensity tested (mean 100 +/− 6 mV/mm). Thus, as expected, cortical AP threshold increases rapidly with decreasing pulse duration (see also DC-chronaxie below); We can conclude that electric field strengths greater than 79 to 120 mV/mm are necessary for significant activation of *quiescent* (see discussion) cortical neurons in slice preparations by 0.5 ms (TMS-like) electric field pulses.

Differing mechanisms of action potential initiation between intracellular current injection and suprathreshold electric field stimulation

In 10 of 26 cells, we observed a transition from regular spiking behavior in response to intracellular current injection, to intrinsic burst spiking (see methods) when the same cell is stimulated by an electric field (Fig. 8A). 4 of these cells were classified as LII/III pyramidal and 6 were classified as LV/VI pyramidal. This data indicates a change in the intrinsic firing pattern of cells, depending on the type of stimulation used.

The firing time of 26 cells in response to 100 ms incrementing steps of electric field and somatic current injection was compared. DC stimulation intensity-time to first AP plots (e.g. strength-duration curves) were constructed for each cell (see Methods), for both stimulation types (Fig. 8A). In 23 out of 26 cells, the DC-chronaxie through electric field stimulation was lower then that of intracellular current injection, resulting in a significant difference between stimulation types (t-test, $p < .01$, Fig. 8B). 8 of these cells were unable to be indentified as a particular cell type. Among LV/VI cells, a significant difference between the DC-chronaxie of electric field stimulation and that of intracellular current injection was evident (n=8, $p < .001$), while for LII/III cells (n=6, $p = .09$) and for interneurons ($p=.07$, n=4) the difference approached significance.

Discussion

To address the basic neural mechanisms of cortical electrotherapy, in the present report we used *in vitro* whole-cell recordings and uniform electric field stimulation. A necessary step toward the rational design of sub- and suprathreshold brain stimulation paradigms is a

systematic and quantitative method for predicting which neuronal elements respond to electric fields; this analysis can then be scaffolded onto theories of network processing and the ultimate therapeutic outcomes.

Relevance of in vitro data to clinical brain stimulation

Several factors concomitantly facilitate the precise characterization of electric field effects *in vitro*, while qualifying how *in vitro* data is used to understand and design clinical electrotherapies. The application of uniform electric fields to brain slice preparations [e.g. [25], 26,39,48,52,54,55,63] results in each cell exposed to an identical 'electrical environment', such that differences in neuronal responses can be attributed (and correlated) directly to differences in neuronal morphological/biophysical characteristics (Supplementary Fig. 1). Only in cases where electric fields induced in the brain for clinical therapies and research are uniform on the scale of a single neuron, as may be the case for non-invasive stimulation or distant cortical electrodes, can our data be used to directly predict neuronal response to the specific 'quasi-uniform' electric field at each location (e.g. cortical layer) in the brain.

In brain slices, the majority of afferents are cut, and intact synapses are inactive compared to the *in vivo* situation [51,62]. These changes affect cellular properties such as resting membrane potential and conductance, as well as AP threshold. Similarly, spontaneous network oscillations, and other forms of 'tonic' system drive, which may modulate neuronal sub- and suprathreshold response [64,65], are absent in brain slices superfused with "normal" ACSF.

In response to *subthreshold* stimulation, in the absence of (by definition) electric-field induced synaptic activation, and ongoing neuronal oscillations (*in vitro*), *neuronal morphology* merits investigation as a predictor of neuronal response. Our morphological reconstructions account for, in part, the inherent cutting of some dendritic processes during brain slice preparation.

Suprathreshold responses integrate the direct neuronal response to the electric field and the cumulative synaptic response by the network. Thus *cell type*, encompassing laminar position, network connectivity, and neuronal morphology merits investigation.

Response to subthreshold fields

It is well established, that in response to subthreshold electric fields, neurons polarize in a compartment specific fashion with compartments oriented towards the anode generally hyperpolarizing and compartments oriented towards the cathode depolarizing [21,25,26,54, 63,66]. Somatic polarization may be reflected as a corresponding change in spontaneous firing rate [24,27,67]. Neuronal cell types with a non-symmetric dendritic morphology are preferentially modulated by the polarity of the electric field [23,24].

Our results indicate that based only on volume-weighted neuronal morphology (without considering cell/compartment specific membrane biophysics) the polarity of cortical neuron somatic membrane polarization by uniform fields can be predicted with high fidelity, and the magnitude of polarization approximated, using the volume-weighted polar histogram coherence vector (described by the mean angle and vector length).

The polar histogram coherence vectors provide a parsimonious model of cortical neuron morphology in relation to electric field induced somatic polarization. Its intuitive applicability, independence of non-linear cellular biophysics, and lower computational overhead gives it merit. This intuitive approach is thus applicable to predict subthreshold polarization from solely morphological data. For example, because the vector length is lower for symmetric cells, (e.g. some interneurons; Fig. 5), the polar histogram model predicts reduced maximum somatic polarization length (λ_p) for such cells compared to larger, more asymmetric (e.g. pyramidal) cells with a higher vector length. The model also predicts that optimal positive and negative

polarization length, for any given cell, is achieved for mean angles of 90° and 270° respectively, aligned with the electric fields. Cells with mean angles perpendicular to the direction of the electric field (0° or 180°) are predicted not to polarize significantly (low λ_p), regardless of vector length.

However, the polar histogram coherence vector model neglects weighting of neuronal segments by their proximity to the soma and distributed cellular biophysics. Indeed, though the dependence of the observed polarization on polar histogram morphological variables is significant ($p < .001$) this parsimonious model does not account for almost half of the observed variance ($r^2 = .41$). Given compartment specific biophysical parameters for each neuron, the 2nd derivative of the extracellular voltage along the membrane [i.e. activating function; 40, 68] would yield more accurate predications (morphological data shall be published on www.neuromorpho.org).

Individually, Layer V pyramids exhibited the highest measured somatic sensitivities to subthreshold fields (polarization lengths, λ_p), and the highest polar histogram vector lengths, a measure of the asymmetry of the volume of neuronal membrane in relation to the soma. Applied *subthreshold* electric field therapies (tDCS, tACS), if quasi-uniform across cortical regions, would thus preferentially polarize Layer V cell somas. Human cortical neurons can be longer than the rat cortical neurons investigated here [62]. However, assuming the ratio of volume between the sum of apical and basal neuronal elements is similar between rat and human cortical neurons, then despite differences in overall size the polar histogram metric would scale accordingly to predict a similar distribution of *somatic* polarization differences across species (Fig. 2).

Distal terminal electric field induced polarization is important to quantify because: a) the maximum polarization is thought to occur at the terminals [21,23,38], and b) dendrite polarization will modulate neuronal processing (e.g. the site of synaptic input [25]. The distal polarization of a symmetrically branching dendritic tree has been modeled [38], in one case with approximately 2.5 times greater polarization at the distal terminal than at the soma [37]. We emphasize that basal and apical dendrites will concomitantly polarize in opposite directions, thus it is incorrect to describe any electric field (experimentally or clinically) as globally de- or hyperpolarizing.

Response to suprathreshold fields, mechanisms of AP initiation

Several lines of evidence suggest that AP initiation in response to uniform electric fields cannot be explained by a simple linear depolarization of the soma to threshold: (1) While the values of subthreshold polarization per unit electric field recorded at the soma linearly correlated to field polarity, in some cells, spiking was initiated with fields of either polarity, or of polarity opposite to the sub-threshold polarization value; (2) The values of subthreshold polarization per unit electric field recorded at the soma, multiplied by the electric field induced firing threshold (expected somatic polarization at threshold electric field) is less than the difference between resting membrane potential and action potential threshold (expected somatic polarization necessary for somatic AP initiation); an extreme example was a cell with a sub-threshold somatic polarization value of 0 $mV*(mV/mm)^{-1}$ and electric field firing threshold of 72 mV/mm; (3) EPSPs were evident in most cells recorded during stimulation, and were dependent on glutamatergic synaptic activity; (4) The DC chronaxie values for electric field stimulation were lower than for intracellular current injection reflecting differing neuronal elements triggering AP initiation for the two stimulation cases [60], and/or synaptic contributions towards electric field induced firing threshold. The spatial profile of stimulation may also impact chronaxie measurements; with neuronal elements charging and summing in parallel during uniform electric field stimulation. Related to this latter point, (5) some cells

that were not categorized as "intrinsically bursting" in response to intracellular current injection (see Methods), exhibited bursting behavior when stimulated by electric fields.

Bursting has been hypothesized as dependent on the opening of hyperpolarization-activated channels of a distal dendritic region (e.g. by inhibitory inputs), while an action potential generated in a depolarized region of the cell back-propagates to this distal hyperpolarized region resulting in dendritic calcium spikes [69–71]. The original action potential and subsequent dendritic spikes may be observed from a somatic recording as a burst response. Incorporating this hypothesis with theory of electric field stimulation (in contrast to intracellular current injection) simultaneously de-and hyperpolarizing distinct neuronal compartments, may be a mechanism for the observed modulation to bursting in response to the electric field.. We have observed modulation of firing to a burst response in pyramidal cells, where distal and basal compartments are electrotonically distant [72].

Response to suprathreshold fields

In coronal *in vitro* brain slices, individual Layer V/VI cells demonstrated the lowest AP threshold in response to 100 ms uniform electric fields. We have found evidence for both direct and orthodromic activation of layer V/VI cells. However, it is important to emphasize that recruitment order is a spectrum across cell types, consistent with a network/orthodromic contribution to activation for most cells. One goal of probing cortical slices with suprathreshold electric fields is to characterize the utility of cortical brain slices as a research tool for suprathreshold non-invasive transcranial stimulation (e.g. TMS). We have recorded a sparse sample of cortical neurons, with 3 of 34 cells exhibiting direct activation (without EPSPs) in response to 100 ms pulses, and an unrelated minority of cells responded to short, TMS-like pulses. Lower stimulator outputs of laterial medial (l–m) TMS coil orientations or any stimulator outputs of posterior-anterior (p-a) TMS are considered only to induce (indirect) i-waves, while greater stimulator output in the l–m orientation is necessary to induce (direct) d-waves [73,74].

Despite experimental differences between *in vitro* uniform electric fields and human cranial stimulation approached, biophysical features governing suprathreshold response (e.g. morphology, cell type, connectivity) should be generalizable. *In vitro*, because all neurons were exposed to a uniform electric field, we demonstrated that differences in suprathreshold response can be attributed to (the uncontrolled variable of) biophysical distinctions of cortical cell types.

In addition, the absolute firing thresholds and recruitment order *in vitro* may be different than during clinical stimulation because of: 1) greater electric field nonuniformities during clinical stimulation, particularly the action potential initiation zones; 2) using *in vitro* preparations, portions of axons are inevitably cut, including corticospinal axons, that have been attributed to d-waves [19,75] and corticocortical afferents linked to the generation of i-waves [74,76]; 3) the square pulse used here leading to differing neuronal activation than the mono- or biphasic waveforms generated by TMS [77], while the pulse lengths used in TMS and TES are much shorter as well; 4) differences in size, length constant, and morphology between human and rat cortical neurons; 5) ongoing network activity (e.g. state dependant activation).

For the reasons noted above, *in vitro*, only a minority of neurons fired in response to 500 μs electric field step pulses with amplitudes up to the maximum possible for our experimental setup, which encompasses the reported range of clinical TMS motor-evoked potential (MEP) threshold amplitudes of 30 to 130 mV/mm [78–80]. In addition, the observed recruitment orders across cortical cell types in response to 100 ms square pulses, may not hold for sub-500 μs pulses probed at even higher intensities than used here, possibly because at this timescale summation of direct electric field polarization and (delayed) EPSP induced polarization is not

possible. Additionally, the capacitance of differing cortical cell types/cellular compartments may change polarization induced by electric fields of varying pulse lengths [81,82].

Towards a mechanistic understanding and rational design of clinical cortical brain stimulation

Which neuronal elements are activated by electrical stimulation are considered to underlie the ultimate behavioral and therapeutic outcomes [29]. Central to this idea is that not all neurons will be equally effected by a given stimulation protocol, and that distinct stimulation protocols target distinct neuronal populations/neuronal compartments. Therefore, determining *which cells are acutely modulated by stimulation is a pivotal first step toward the rational design of electrotherapies*: however, this is only a first step toward the complex analysis of how electrical stimulation affects information processing, synaptic plasticity, network function and ultimately behavior. Conversely, network activity may affect both subthreshold polarization sensitivity (polarization length, λ_p) and suprathreshold recruitment order. The present study addressed only the first step by taking advantage of the isolated brain slice preparation. This section addresses how to extend this insight in the context of neuronal processing.

Development of subthreshold stimulation paradigms should consider the polarization of specific neuronal compartments (such as the soma or specific dendritic terminals), in the context of their roles in ongoing neuronal processing. For the range of electric fields induced by typical subthreshold clinical electrotherapies (e.g. tDCS), the predicted membrane polarization is on the order of mV; even at the tufts of the largest cortical neurons [37]. How can such relatively small polarizations lead to significant functional changes in the brain? When considered in the context of ongoing activity, we have shown that acutely, weak fields may be amplified at the single cell [48] and network [65] levels, through changes in spike timing. In addition to these acute “amplification” mechanisms, it is necessary to characterize the plastic effects of electrical stimulation protocols; for example *prolonged* weak depolarization (>10 minutes), is thought to lead to plastic changes as observed during tDCS [83–85]..

The ultimate goal of rational electrotherapy is to promote changes in network function that alleviate behavioral symptoms while minimizing disruption of cognitive function. The characterization of cellular responses to stimulation is a necessary but incremental step toward this goal. In summary, the present study addresses the importance of cortical neuronal morphology and cortical cell type during sub- and suprathreshold electric field stimulation. These data are a necessary step toward a mechanistic understanding of clinical cortical electrotherapy, and the design of more targeted (e.g. focal, fewer side-effects, longer lasting) brain stimulation strategies.

Supplementary Material

Refer to Web version on PubMed Central for supplementary material.

Acknowledgments

Abhishek Datta, Reem Khalil, Jonathan B. Levitt, and Lucas C. Parra of the City College of New York; Zhi-De Deng and Angel V. Peterchev of Columbia University, Boris Heifets and Pablo Castillo of Albert Einstein College of Medicine of Yeshiva University; Sébastien J. Thuault and Stephen A. Siegelbaum of Columbia University; Natascia Vedovato and David C. Gadsby of Rockefeller University; Jimmy K. Duong of the Irving Institute Biostatistics Consultation Service; Adair Oesterle of Sutter Instruments. This work was supported in part by the NIH, the Wallace H. Coulter Foundation, and PSC-CUNY.

References

1. Liebetanz D, et al. Anticonvulsant effects of transcranial direct-current stimulation (tDCS) in the rat cortical ramp model of focal epilepsy. Epilepsia 2006;47(7):1216–24. [PubMed: 16886986]
2. George MS, Lisanby SH, Sackeim HA. Transcranial magnetic stimulation: applications in neuropsychiatry. Arch Gen Psychiatry 1999;56(4):300–11. [PubMed: 10197824]
3. Avery DH, et al. A controlled study of repetitive transcranial magnetic stimulation in medication-resistant major depression. Biol Psychiatry 2006;59(2):187–94. [PubMed: 16139808]
4. Boggio PS, et al. Effects of transcranial direct current stimulation on working memory in patients with Parkinson's disease. J Neurol Sci 2006;249(1):31–8. [PubMed: 16843494]
5. Webster BR, Celnik PA, Cohen LG. Noninvasive brain stimulation in stroke rehabilitation. NeuroRx 2006;3(4):474–81. [PubMed: 17012061]
6. Fregni F, et al. A sham-controlled, phase II trial of transcranial direct current stimulation for the treatment of central pain in traumatic spinal cord injury. Pain 2006;122(1–2):197–209. [PubMed: 16564618]
7. Uy J, Ridding MC. Increased cortical excitability induced by transcranial DC and peripheral nerve stimulation. J Neurosci Methods 2003;127(2):193–7. [PubMed: 12906948]
8. Marshall L, et al. Boosting slow oscillations during sleep potentiates memory. Nature 2006;444(7119): 610–3. [PubMed: 17086200]
9. Fregni F, et al. Anodal transcranial direct current stimulation of prefrontal cortex enhances working memory. Exp Brain Res 2005;166(1):23–30. [PubMed: 15999258]
10. Kincses TZ, et al. Facilitation of probabilistic classification learning by transcranial direct current stimulation of the prefrontal cortex in the human. Neuropsychologia 2004;42(1):113–7. [PubMed: 14615081]
11. Amassian VE, et al. Modelling magnetic coil excitation of human cerebral cortex with a peripheral nerve immersed in a brain-shaped volume conductor: the significance of fiber bending in excitation. Electroencephalogr Clin Neurophysiol 1992;85(5):291–301. [PubMed: 1385089]
12. Miranda PC, Lomarev M, Hallett M. Modeling the current distribution during transcranial direct current stimulation. Clin Neurophysiol 2006;117(7):1623–9. [PubMed: 16762592]
13. Krings T, et al. Functional magnetic resonance imaging and transcranial magnetic stimulation: complementary approaches in the evaluation of cortical motor function. Neurology 1997;48(5): 1406–16. [PubMed: 9153482]
14. Wassermann EM, et al. Locating the motor cortex on the MRI with transcranial magnetic stimulation and PET. Neuroimage 1996;3(1):1–9. [PubMed: 9345470]
15. Komssi S, et al. Excitation threshold of the motor cortex estimated with transcranial magnetic stimulation electroencephalography. Neuroreport 2007;18(1):13–6. [PubMed: 17259853]
16. Normann RA, et al. A neural interface for a cortical vision prosthesis. Vision Res 1999;39(15):2577–87. [PubMed: 10396626]
17. Badi AN, et al. A technique for implantation of a 3-dimensional penetrating electrode array in the modiolar nerve of cats and humans. Arch Otolaryngol Head Neck Surg 2002;128(9):1019–25. [PubMed: 12220205]
18. Esser SK, Hill SL, Tononi G. Modeling the effects of transcranial magnetic stimulation on cortical circuits. J Neurophysiol 2005;94(1):622–39. [PubMed: 15788519]
19. Pascual-Leone A, et al. Responses to rapid-rate transcranial magnetic stimulation of the human motor cortex. Brain 1994;117(Pt 4):847–58. [PubMed: 7922470]
20. Takano B, et al. Short-term modulation of regional excitability and blood flow in human motor cortex following rapid-rate transcranial magnetic stimulation. Neuroimage 2004;23(3):849–59. [PubMed: 15528085]
21. Maccabee PJ, et al. Magnetic coil stimulation of straight and bent amphibian and mammalian peripheral nerve in vitro: locus of excitation. J Physiol 1993;460:201–19. [PubMed: 8487192]
22. Amassian VE, et al. The polarity of the induced electric field influences magnetic coil inhibition of human visual cortex: implications for the site of excitation. Electroencephalogr Clin Neurophysiol 1994;93(1):21–6. [PubMed: 7511518]

23. Chan CY, Hounsgaard J, Nicholson C. Effects of electric fields on transmembrane potential and excitability of turtle cerebellar Purkinje cells in vitro. J Physiol 1988;402:751–71. [PubMed: 3236254]
24. Hern JEC, et al. Selective Excitation of Cortifgugal Neurones by Surface-Anodal Stimulation of the Baboon's Motor Cortex. J Physiol 1962;161:73–90. [PubMed: 13906736]
25. Bikson M, et al. Effects of uniform extracellular DC electric fields on excitability in rat hippocampal slices in vitro. J Physiol 2004;557(Pt 1):175–90. [PubMed: 14978199]
26. Chan CY, Nicholson C. Modulation by applied electric fields of Purkinje and stellate cell activity in the isolated turtle cerebellum. J Physiol 1986;371:89–114. [PubMed: 3701658]
27. Purpura DP, McMurtry JG. Intracellular Activities and Evoked Potential Changes During Polarization of Motor Cortex. J Neurophysiol 1965;28:166–85. [PubMed: 14244793]
28. Lopez L, et al. Multimodal characterization of population responses evoked by applied electric field in vitro: extracellular potential, magnetic evoked field, transmembrane potential, and current-source density analysis. J Neurosci 1991;11(7):1998–2010. [PubMed: 2066771]
29. Ranck JB Jr. Which elements are excited in electrical stimulation of mammalian central nervous system: a review. Brain Res 1975;98(3):417–40. [PubMed: 1102064]
30. Wagner T, Valero-Cabre A, Pascual-Leone A. Noninvasive human brain stimulation. Annu Rev Biomed Eng 2007;9:527–65. [PubMed: 17444810]
31. Gatter KC, Sloper JJ, Powell TP. The intrinsic connections of the cortex of area 4 of the monkey. Brain 1978;101(3):513–41. [PubMed: 101281]
32. Miranda PC, Hallett M, Basser PJ. The electric field induced in the brain by magnetic stimulation: a 3-D finite-element analysis of the effect of tissue heterogeneity and anisotropy. IEEE Trans Biomed Eng 2003;50(9):1074–85. [PubMed: 12943275]
33. Wagner T, et al. Transcranial direct current stimulation: a computer-based human model study. Neuroimage 2007;35(3):1113–24. [PubMed: 17337213]
34. Datta A, et al. Transcranial current stimulation focality using disc and ring electrode configurations: FEM analysis. J Neural Eng 2008;5(2):163–74. [PubMed: 18441418]
35. Rattay F. Analysis of models for extracellular fiber stimulation. IEEE Trans Biomed Eng 1989;36 (7):676–82. [PubMed: 2744791]
36. Nagarajan SS, Durand DM, Warman EN. Effects of induced electric fields on finite neuronal structures: a simulation study. IEEE Trans Biomed Eng 1993;40(11):1175–88. [PubMed: 8307602]
37. Hause, L. A mathematical model for transmembrane potentials secondary to extracellular fields. In: Sances, J.; Larson, S., editors. Electroanaesthesia: Biomedical and Biophysical Studies. Academic; New York: 1975. p. 176-200.
38. Tranchina D, Nicholson C. A model for the polarization of neurons by extrinsically applied electric fields. Biophys J 1986;50(6):1139–56. [PubMed: 3801574]
39. Svirskis G, et al. Electrotonic measurements by electric field-induced polarization in neurons: theory and experimental estimation. Biophys J 1997;73(6):3004–15. [PubMed: 9414215]
40. McIntyre CC, Grill WM. Excitation of central nervous system neurons by nonuniform electric fields. Biophys J 1999;76(2):878–88. [PubMed: 9929489]
41. Plonsey R, Barr RC. Electric field stimulation of excitable tissue. IEEE Eng Med Biol Mag 1998;17 (5):130–7. [PubMed: 9770615]
42. Plonsey R, Altman KW. Electrical stimulation of excitable cells-a model approach. Proceedings of the IEEE 1988;76(9):1122–1129.
43. Rotem A, Moses E. Magnetic stimulation of one-dimensional neuronal cultures. Biophys J 2008;94 (12):5065–78. [PubMed: 18326634]
44. Valero-Cabre A, et al. Impact of repetitive transcranial magnetic stimulation of the parietal cortex on metabolic brain activity: a 14C-2DG tracing study in the cat. Exp Brain Res 2005;163(1):1–12. [PubMed: 15688174]
45. Durand DM. Suppression and control of epileptiform activity by electrical stimulation: a review. Proc IEEE 2001;89:1065–1082.
46. Roth BJ. Mechanisms for electrical stimulation of excitable tissue. Crit Rev Biomed Eng 1994;22(3–4):253–305. [PubMed: 8598130]

47. Brumberg JC, Nowak LG, McCormick DA. Ionic mechanisms underlying repetitive high-frequency burst firing in supragranular cortical neurons. J Neurosci 2000;20(13):4829–43. [PubMed: 10864940]
48. Radman T, et al. Spike timing amplifies the effect of electric fields on neurons: implications for endogenous field effects. J Neurosci 2007;27(11):3030–6. [PubMed: 17360926]
49. Ramos RL, Tam DM, Brumberg JC. Physiology and morphology of callosal projection neurons in mouse. Neuroscience 2008;153(3):654–63. [PubMed: 18424008]
50. Yang CR, Seamans JK, Gorelova N. Electrophysiological and morphological properties of layers V–VI principal pyramidal cells in rat prefrontal cortex in vitro. J Neurosci 1996;16(5):1904–21. [PubMed: 8774458]
51. McCormick DA, et al. Comparative electrophysiology of pyramidal and sparsely spiny stellate neurons of the neocortex. J Neurophysiol 1985;54(4):782–806. [PubMed: 2999347]
52. Deans JK, Powell AD, Jefferys JG. Sensitivity of coherent oscillations in rat hippocampus to AC electric fields. J Physiol 2007;583(Pt 2):555–65. [PubMed: 17599962]
53. Ghai RS, Bikson M, Durand DM. Effects of applied electric fields on low-calcium epileptiform activity in the CA1 region of rat hippocampal slices. J Neurophysiol 2000;84(1):274–80. [PubMed: 10899202]
54. Francis JT, Gluckman BJ, Schiff SJ. Sensitivity of neurons to weak electric fields. J Neurosci 2003;23(19):7255–61. [PubMed: 12917358]
55. Gluckman BJ, et al. Electric field suppression of epileptiform activity in hippocampal slices. J Neurophysiol 1996;76(6):4202–5. [PubMed: 8985916]
56. Gluckman BJ, et al. Adaptive electric field control of epileptic seizures. J Neurosci 2001;21(2):590–600. [PubMed: 11160438]
57. Brumberg JC, Hamzei-Sichani F, Yuste R. Morphological and physiological characterization of layer VI corticofugal neurons of mouse primary visual cortex. J Neurophysiol 2003;89(5):2854–67. [PubMed: 12740416]
58. Rocco MM, Brumberg JC. The sensorimotor slice. J Neurosci Methods 2007;162(1–2):139–47. [PubMed: 17307257]
59. Ramos RL, et al. Cytoarchitecture and transcriptional profiles of neocortical malformations in inbred mice. Cereb Cortex 2008;18(11):2614–28. [PubMed: 18308707]
60. Nowak LG, Bullier J. Axons, but not cell bodies, are activated by electrical stimulation in cortical gray matter. I. Evidence from chronaxie measurements. Exp Brain Res 1998;118(4):477–88. [PubMed: 9504843]
61. Bostock H. The strength-duration relationship for excitation of myelinated nerve: computed dependence on membrane parameters. J Physiol 1983;341:59–74. [PubMed: 6312032]
62. Meyer G. Forms and spatial arrangement of neurons in the primary motor cortex of man. J Comp Neurol 1987;262(3):402–28. [PubMed: 3655019]
63. Jefferys JG. Influence of electric fields on the excitability of granule cells in guinea-pig hippocampal slices. J Physiol 1981;319:143–52. [PubMed: 7320909]
64. Lakatos P, et al. An oscillatory hierarchy controlling neuronal excitability and stimulus processing in the auditory cortex. J Neurophysiol 2005;94(3):1904–11. [PubMed: 15901760]
65. Parra LC, Bikson M. Model of the effect of extracellular fields on spike time coherence. Conf Proc IEEE Eng Med Biol Soc 2004;6:4584–7. [PubMed: 17271327]
66. Delgado-Lezama R, Perrier JF, Hounsgaard J. Local facilitation of plateau potentials in dendrites of turtle motoneurones by synaptic activation of metabotropic receptors. J Physiol 1999;515(Pt 1):203–7. [PubMed: 9925889]
67. Terzuolo CA, Bullock TH. Measurement of Imposed Voltage Gradient Adequate to Modulate Neuronal Firing. Proc Natl Acad Sci U S A 1956;42(9):687–94. [PubMed: 16589932]
68. McIntyre CC, Grill WM. Selective microstimulation of central nervous system neurons. Ann Biomed Eng 2000;28(3):219–33. [PubMed: 10784087]
69. Izhikevich, E. Neuroscience: Geometry of Excitability and Bursting. MIT Press; 2005. Dynamical Systems.

70. Lesica NA, Stanley GB. Encoding of natural scene movies by tonic and burst spikes in the lateral geniculate nucleus. J Neurosci 2004;24(47):10731–40. [PubMed: 15564591]
71. Lu SM, Guido W, Sherman SM. Effects of membrane voltage on receptive field properties of lateral geniculate neurons in the cat: contributions of the low-threshold Ca2+ conductance. J Neurophysiol 1992;68(6):2185–98. [PubMed: 1337104]
72. Larkman AU, et al. Dendritic morphology of pyramidal neurones of the visual cortex of the rat. IV: Electrical geometry. J Comp Neurol 1992;323(2):137–52. [PubMed: 1401253]
73. Brocke J, et al. Transcranial magnetic and electrical stimulation compared: does TES activate intracortical neuronal circuits? Clin Neurophysiol 2005;116(12):2748–56. [PubMed: 16256428]
74. Patton HD V, Amassian E. Single and multiple-unit analysis of cortical stage of pyramidal tract activation. J Neurophysiol 1954;17(4):345–63. [PubMed: 13175052]
75. Rothwell J, et al. Transcranial electrical stimulation of the motor cortex in man: further evidence for the site of activation. J Physiol 1994;481(Pt 1):243–50. [PubMed: 7853247]
76. Nakamura H, et al. Intracortical facilitation and inhibition after transcranial magnetic stimulation in conscious humans. J Physiol 1997;498(Pt 3):817–23. [PubMed: 9051592]
77. Sommer M, et al. Neuronal tissue polarization induced by repetitive transcranial magnetic stimulation? Neuroreport 2002;13(6):809–11. [PubMed: 11997692]
78. Epstein CM, et al. Localizing the site of magnetic brain stimulation in humans. Neurology 1990;40 (4):666–70. [PubMed: 2320243]
79. Rudiak D, Marg E. Finding the depth of magnetic brain stimulation: a reevaluation. Electroencephalogr Clin Neurophysiol 1994;93(5):358–71. [PubMed: 7525244]
80. Thielscher A, Kammer T. Linking physics with physiology in TMS: a sphere field model to determine the cortical stimulation site in TMS. Neuroimage 2002;17(3):1117–30. [PubMed: 12414254]
81. Peterchev AV, Jalinous R, Lisanby SH. A transcranial magnetic stimulator inducing near-rectangular pulses with controllable pulse width (cTMS). IEEE Trans Biomed Eng 2008;55(1):257–66. [PubMed: 18232369]
82. Tehovnik EJ, et al. Direct and indirect activation of cortical neurons by electrical microstimulation. J Neurophysiol 2006;96(2):512–21. [PubMed: 16835359]
83. Nitsche MA, et al. Modulation of cortical excitability by weak direct current stimulation--technical, safety and functional aspects. Suppl Clin Neurophysiol 2003;56:255–76. [PubMed: 14677403]
84. Nitsche MA, et al. Pharmacological modulation of cortical excitability shifts induced by transcranial direct current stimulation in humans. J Physiol 2003;553(Pt 1):293–301. [PubMed: 12949224]
85. Nitsche MA, Paulus W. Excitability changes induced in the human motor cortex by weak transcranial direct current stimulation. J Physiol 2000;527(Pt 3):633–9. [PubMed: 10990547]

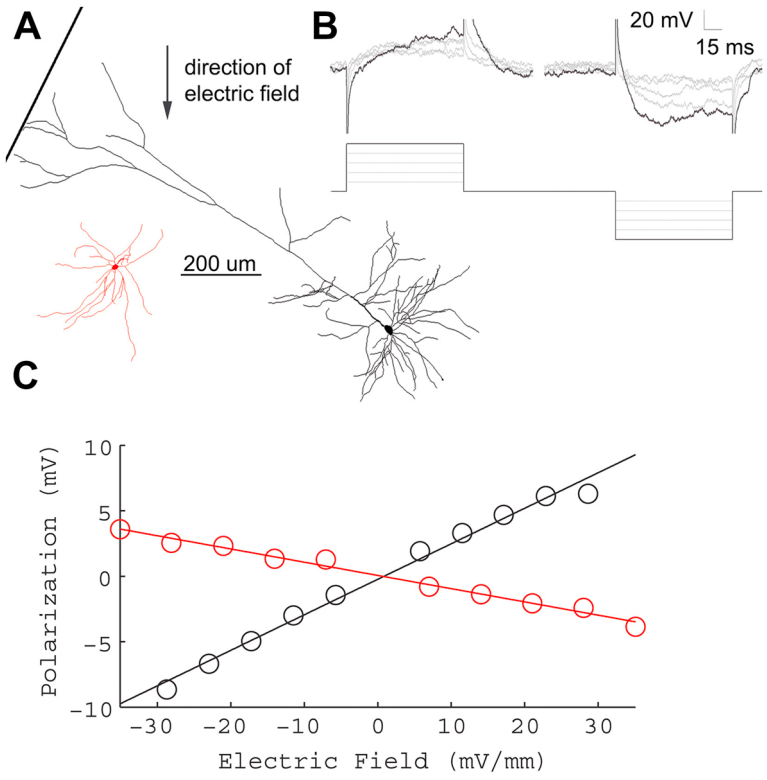

Figure 1.

Sub-threshold electric fields polarize cortical neuronal soma linearly. ***A,*** Example morphological reconstruction of a L5 pyramidal neuron (black), and L5 fast-spiking interneuron (red) ***B,*** Incrementing electric field steps of 5.8 mV/mm (bottom) linearly polarize cell soma (top). Reconstructions shown are from L5 regular spiking pyramidal neuron of *A* (top). ***C,*** Summary of the polarization per electric field for the neurons shown in *A*. The slope of the fitted line determines the sub-threshold field polarization sensitivity for each neuron. LV pyramidal neuron (black) = .27 mV*(mV/mm)$^{-1}$, LV fast-spiking interneuron (red) = −. 02 mV*(mV/mm)$^{-1}$.

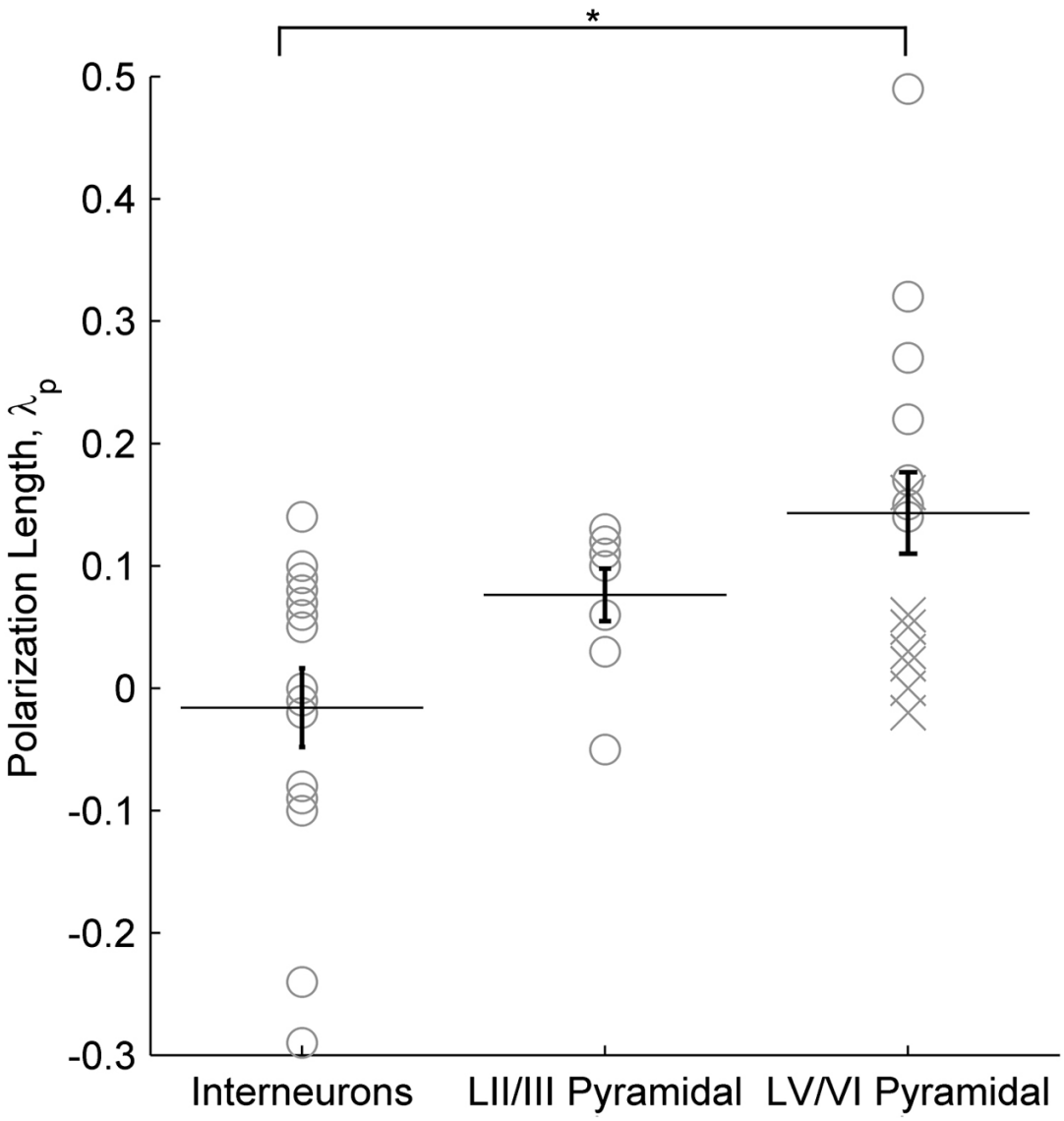

Figure 2.

Cortical cell type polarization sensitivity. The polarization length, λ_p (mm), an indicator of mV or polarization per unit electric field applied (mV/mm), is shown according to cell type. Asterisk denotes significant difference (T-test) found between LV/VI pyramidal neurons and interneurons across layers. Points labeled as an "X" are neurons with cut dendritic trees that have still been included in all analyses.

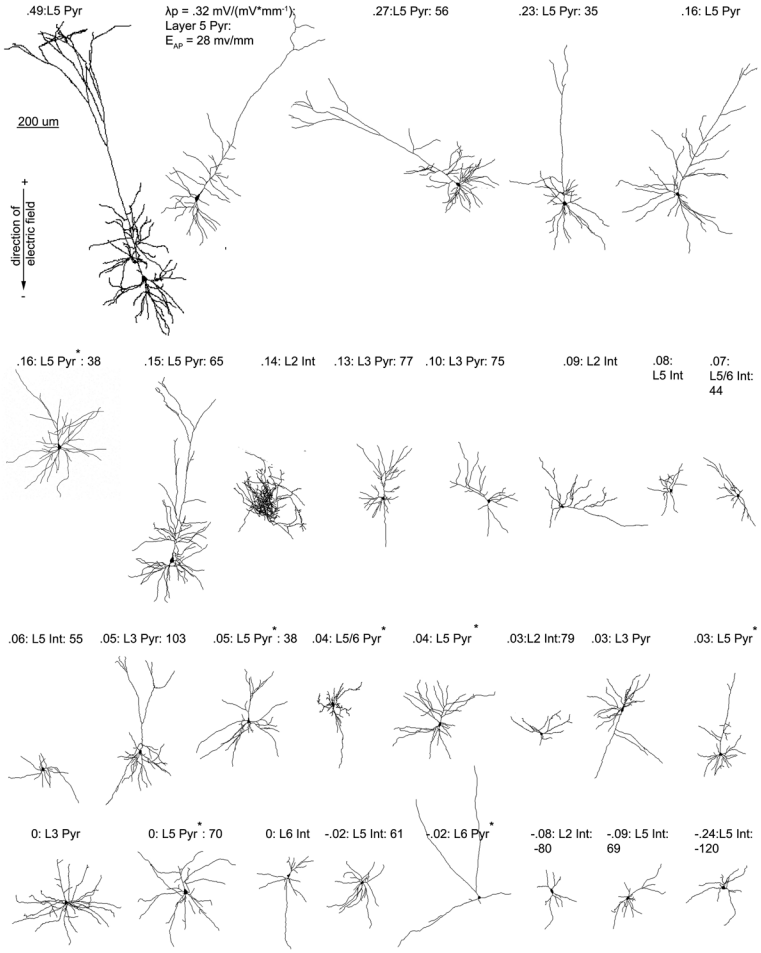

Figure 3.

Cortical neuron morphological reconstructions in order of electric field induced somatic polarization sensitivity. 3 items are listed for each cell, electric field induced somatic polarization length, λ_p (mm), an indicator of mV of polarization per unit electric field applied (mV/mm), layer, and cell type (pyramidal or interneuron); and if tested for that cell, electric field induced firing threshold. An asterisk next to the label for cell type denotes a neuron with a cut dendritic tree, that has still been included in all analyses.

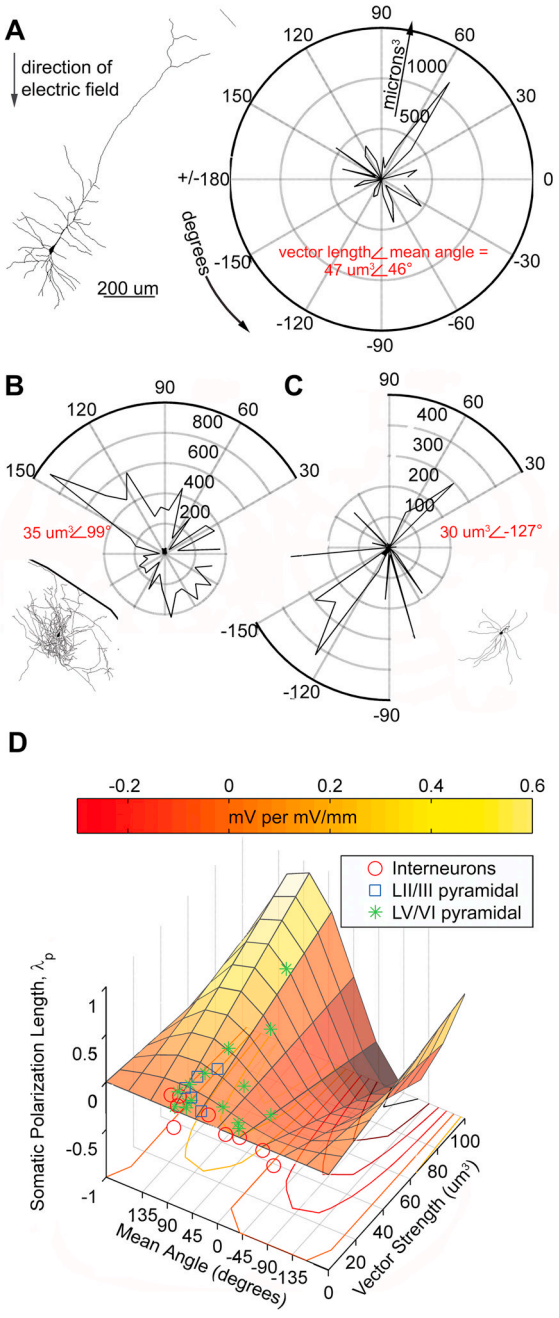

Figure 4.

Polar histogram coherence vector: Neuronal morphology predicts somatic polarization sensitivity to sub-threshold electric fields. ***A–C,*** Example tracings and corresponding volume-weighted polar histograms of (*A)* LV regular spiking pyramidal neuron with electric field The polarization length, λ_p (mm), an indicator of mV or polarization per unit electric field applied (mV/mm), = .32 mm, the polar histogram can be summarized by the variables: mean angle = 46° and vector length = 47 um^3, representing the center of mass of the histogram; (*B)* LII fast spiking interneuron with polarization length = .14 mm, mean angle = 99° and vector length = 35 um^3; and (*C)* LV fast spiking interneuron with polarization length = −.02 mm, mean angle = −127° and vector length = 30 um^3. ***D,*** Summary plot of all neurons recorded and traced, with

polar histogram coherence vectors as predictors of somatic polarization per electric field for each neuron. The colored plane is the statistically significant, best fit regression to the equation: polarization length = m*sine(mean angle)*vector length ($p < .02$, $r^2 = .41$, n=30).

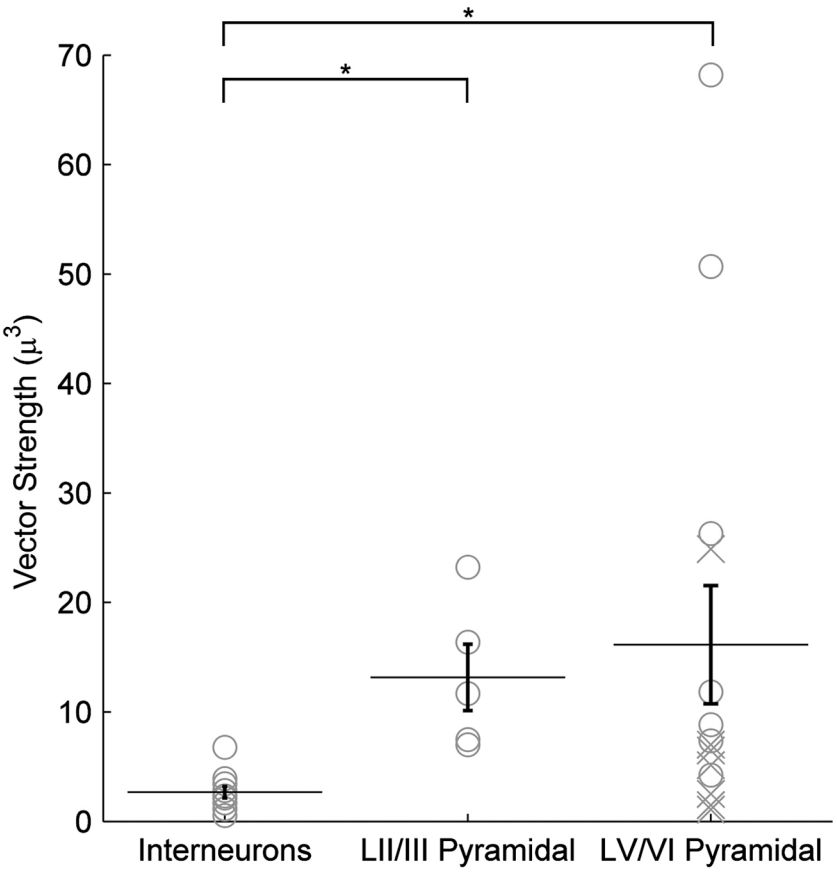

Figure 5.

Cortical cell type vector lengths. The polar histogram (Fig. 4) summary variable vector length, is shown according to cell type. Asterisk denotes significant difference (T-test) found between as interneurons across layers and both LV/VI pyramidal neurons, and LII/III pyramidal neurons as well. Points labeled as an "X" are neurons with cut dendritic trees that have still been included in all analyses.

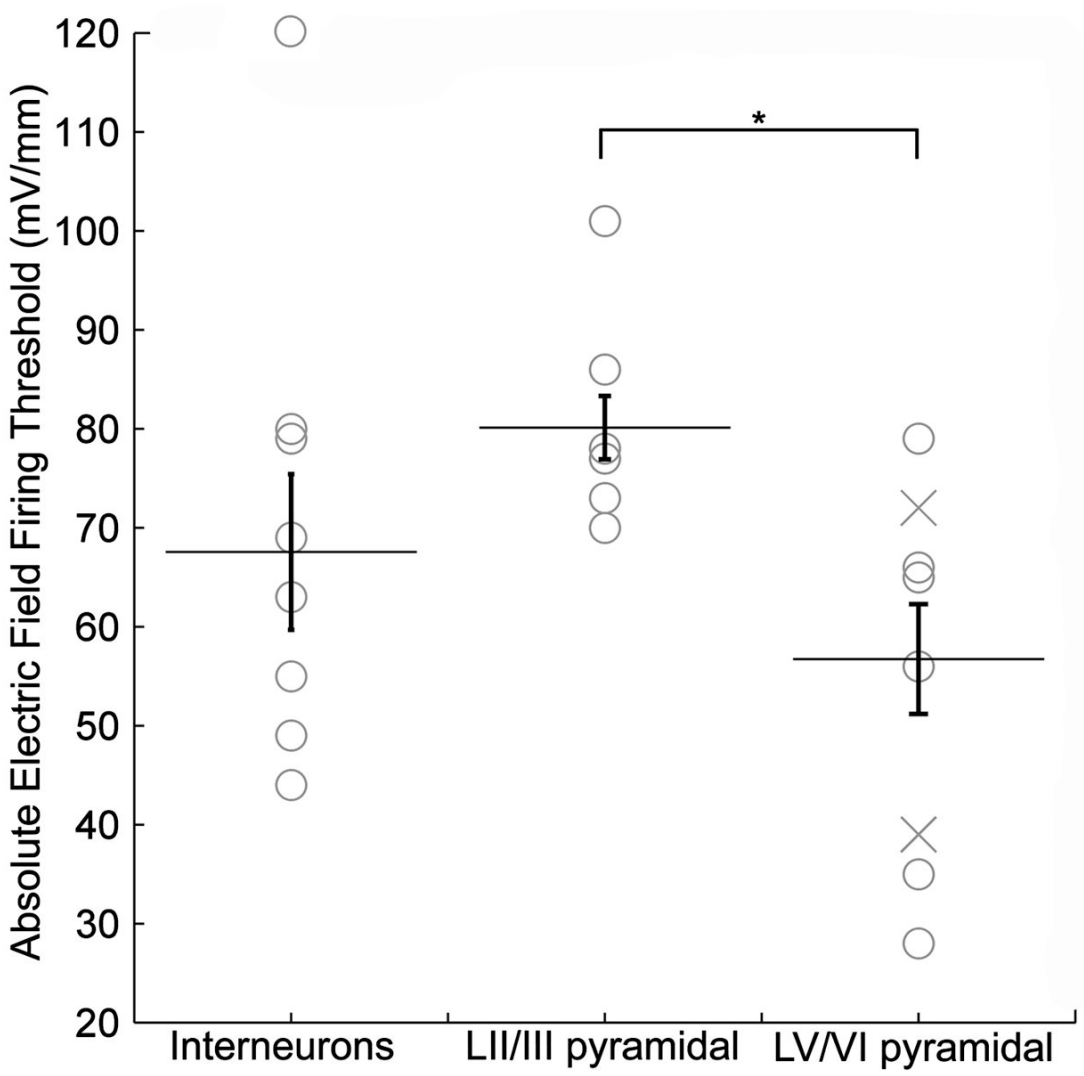

Figure 6.
Cortical cell type electric field firing thresholds. The minimum absolute electric field firing threshold, in response to 100 ms incrementing electric field steps, is shown according to cell type. Asterisk denotes significant difference (T-test) found between LV/VI pyramidal neurons, and both LII/III pyramidal neurons as well as interneurons across layers.

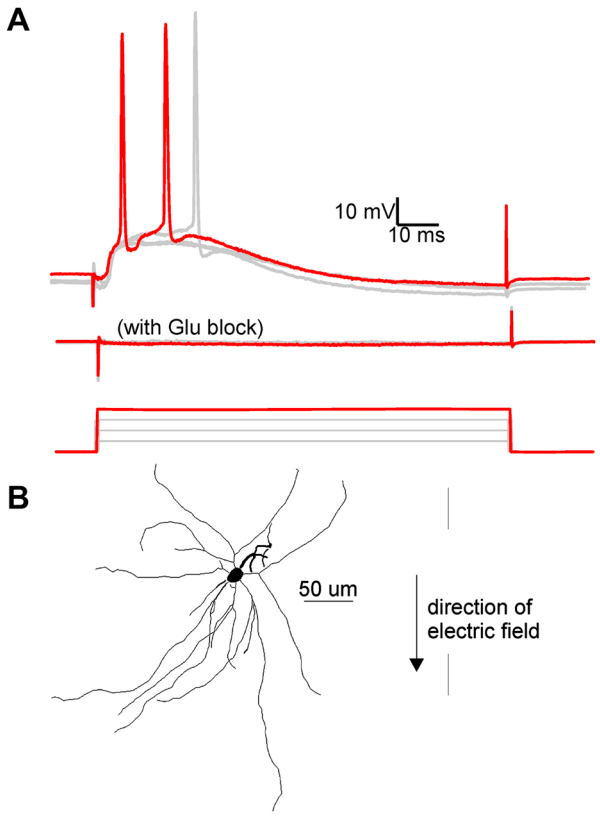

Figure 7.

Electric field induced EPSPs are reduced by bath application of CNQX and APV. ***A,*** Overlay of the response to electric field steps of increasing intensity. *Top*: Recorded intracellular voltage response to electric field steps of 51, 57, 63, and 70 (red trace) mV/mm. Note 63 and 70 mV/mm electric field steps induced action potentials. *Middle*: Voltage response to the same field intensities after 15 minute bath application of 20 μM CNQX and 50 μM APV. *Bottom:* Applied electric field waveforms. ***B,*** Tracing of L5 fast-spiking interneuron described in ***A***.

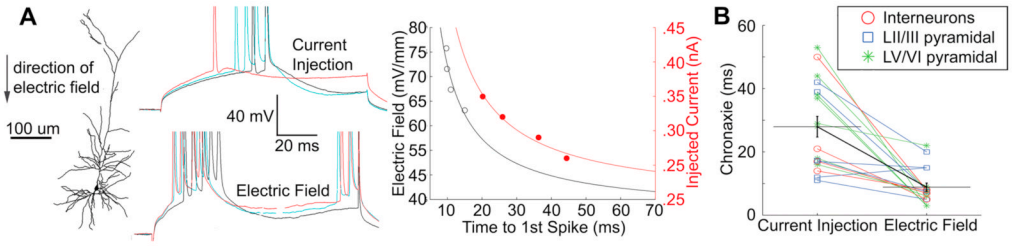

Figure 8.

Time to 1st spike-strength of stimulation chronaxie measurements are lower for electric field stimulation than somatic intracellular current injection. ***A,*** Example morphological reconstruction of a L5 intrinsic bursting pyramidal neuron with transmembrane polarization in response to successive steps of intracellular current injection (top), and electric field stimulation (bottom). Note modulation of firing pattern from regular spiking (top, current injection), to intrinsic bursting (bottom, field stimulation). Summary plot (right), of the time to first spike in response to electric field stimulation (left axis, black) and injected current (right axis, red). The solid lines are best fit curves to y=1/(time to first spike). ***B,*** Comparison of chronaxies, for current injection and electric field stimulation, for each recorded neuron. Statistically significant difference ($p < .01$) between stimulation methods for all cells.